Determination of dynamic rock strength to assess blasting efficiency

Conference Paper · September 2013

CITATION
1

READS
204

5 authors, including:

Frederic Pellet
MINES ParisTech
113 PUBLICATIONS **894** CITATIONS
SEE PROFILE

Kien Van Dạng
Hanoi University of Mining and Geology
6 PUBLICATIONS **4** CITATIONS
SEE PROFILE

Rock Mechanics for Resources, Energy and Environment – Kwaśniewski & Łydżba (eds)
© 2013 Taylor & Francis Group, London, ISBN 978-1-138-00080-3

Determination of dynamic rock strength to assess blasting efficiency

F.L. Pellet, V.K. Dang, C. Baumont, M. Dusseux & G.J. Huang
INSA-University of Lyon, France

ABSTRACT: Dynamic tests using the Split Hopkinson Pressure Bar test (SHPB) were conducted on granite specimens in order to study the efficiency of the drill and blast method and the environmental impact of the excavation of a tunnel in urban areas. The tests were performed at different strain rates of loading corresponding to variable energy levels. Compared to the static uniaxial strength, the dynamic strength of the rock was found to be much higher. The dynamic strength clearly increases with the strain rate of the loading but decreases with the duration of load application. The same conclusions can be drawn for the Young's modulus. Using the experimental results, the strength parameters of the rock were back calibrated using a Finite Element model of the test; preliminary numerical simulations of SHPB tests gave good results. These results can therefore be used to correlate the blasting load to the damage observed in the tunnel during excavation.

1 INTRODUCTION

It has long been known that rock materials behave quite differently under dynamic loadings compared to static loading. Recent studies (Bohloli 1997, Zhou et al. 2012) showed that the Unconfined Compressive Strength (UCS) of rock increases when the loading pulse value increases.

In the present paper, the results of an experimental program performed on Lavasan granite in dynamic loading are presented and compared with static loading tests results (Pellet et al. 2011). This program was conceived to assess the efficiency of the drill and blast excavation method as well as to evaluate the environmental impact of tunnel excavation in an urban area.

2 EXPERIMENTAL PROGRAM

2.1 *Experimental set up for SHPB test*

The Split Hopkinson Pressure Bar test (SHPB) was developed by Kolsky (1949) as a modification of the Hopkinson pressure bar test (Hopkinson 1914). Several studies have been carried out with this equipment on different materials (Forquin et al. 2010, Johnson 2010, Kaiser 1998, Weimin and Jinyu 2009).

The SHPB system is composed of two axial bars (input bar and output bar) and a striker launched by a gas gun. Figure 1 shows a general view of SHPB while Figure 2 presents a schematic of the device.

A short cylindrical specimen is installed between the two main bars. The impact between the striker and the input bar generates a compressive wave (loading wave and unloading waves) which is the output to the specimen.

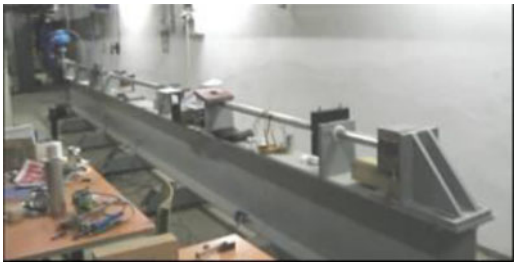

Figure 1. General view of the Split Hopkinson Pressure Bar (SHPB) device in the University of Lyon.

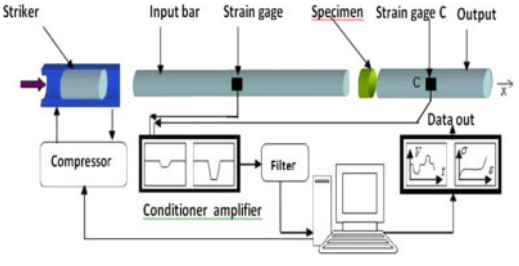

Figure 2. Diagram of the Split Hopkinson Bar Pressure (SHPB) test facility.

The main objective of the SHPB experiments is to perform indirect strain measurements: strains are measured in the bars rather than directly in the specimen. Strain gauges give the values of the strike, the reflected and output strain waves in the bars. From these measurements, the values of the forces and displacements (stress and strain) can be determined at any point along the bars and the specimen at any time.

Table 1. Physical and mechanical properties of Lavasan granite.

Bulk specific gravity	(g/cm^3)	2.65
Porosity	(%)	1.0
P-wave velocity	(m/sec)	3994 ± 35
S-wave velocity	(m/sec)	2550 ± 20
Poisson's ratio	–	0.25
Young's modulus	[GPa]	45 ± 5
UCS	[MPa]	148 ± 15

2.2 *Rock under study*

Tests were performed on Lavasan granite; this has been extensively studied (Keshavarz et al. 2008, Keshavarz et al. 2009). The previous experimental investigations consisted mostly of static uniaxial compression tests with acoustic emission records. Prior to the SHPB tests, the physical properties and the sonic wave velocities (V_p and V_s) of each specimen were measured. The mechanical and physical properties of this granite are summarized in Table 1.

2.3 *Tests preparation*

For each SHPB test the following data were determined and recorded:

- Distance of each strain gauge pair from the strike/specimen bar interface,
- Orientation of the strain gauge pair (axial or circumferential),
- Length of the striker bar,
- Gain of each amplifier determined by shunt calibration,
- Elapsed time for the striker bar to cross the laser timer distance,
- Photograph of the specimen bar before and after impact,
- Additional notes including any damaged gauges and the damage distances,
- Gas gun firing pressure.

The specimen was aligned to the input bar axis using a flashlight and adjusting the support wires until no light could be seen at the interface. The data logger was set to the number of channels to be read. The trigger voltage level for the incident gauges was determined by practice and was set depending on the velocity of the striker bar.

The raw data files consist of ordered pairs of time and voltage for each gauge; these basic time-voltage data sets are used for all subsequent data reductions. Mathematical computations such as zeroing, converting the voltage to strain, time-shifting the reflected wave, super positioning of the incident and reflected waves, calculation of the strain and stress at the interface, and calculation of the loading and unloading strain rate of a wave were facilitated. The data processing involved the following basic steps, some of which are explained in more detail in the following subsections (Johnson 2010):

- Zero the data by subtracting the initial voltage reading from each channel,
- Time-shift the reflected wave in the input bar data,
- Convert zeroed voltage to strain for each channel,
- Calculate stress and strain applied to the specimen bar,
- Tabulate the arrival time, peak strain and plastic strain for each channel.

3 MEASURED AND CONTROLLED PARAMETERS

Measuring the deformation of both the input bar and the output bar allows the applied force, the deformation and the strain rate of the specimen to be obtained. The possibility of obtaining additional measurements includes the displacement of targets using a dynamic strain gauge. A video recording was produced using a fast camera (Phantom V4).

3.1 *Time-shift of the reflected wave*

The incident wave passes through the strain gages near the center of the bar and continues to the interface between the incident bar and specimen. At the interface, part of the wave is transmitted to the specimen bar and part is reflected back into the input bar. Therefore a single channel of data contains both the incident and reflected waves. The start or "zero" of the reflected wave must be determined in order to isolate it from the single channel of data. The time difference or time-shift of the reflected wave must be computed before the incident and reflected strain waves can be superimposed. The time-shift of the reflected wave (Δt_R) is the time required for the wave to travel from the gauge to the interface and return. The time-shift for the reflected incident stress wave is:

$$\Delta t_R = \frac{2l}{c} \tag{1}$$

where c is the sonic wave velocity in the input bar, l is distance from the center of the strain gauge pair on the input bar to the incident bar – specimen interface.

The experimental measurements confirm that the wave velocity in the input bar is in close agreement with that calculated by its elastic modulus and density using the following equation:

$$c = \sqrt{\frac{E}{\rho}} \tag{2}$$

where E is the elastic modulus of the bar or of the specimen (MPa), ρ is the density of the bars or of the specimen (N/m^3).

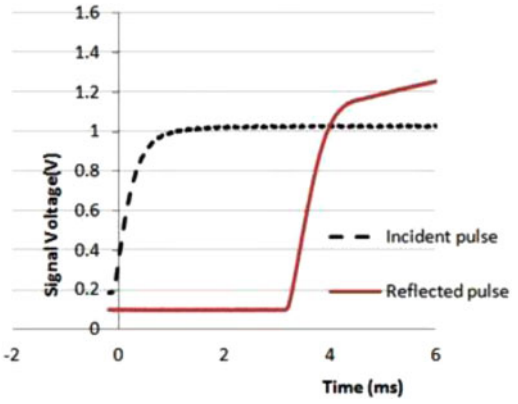

Figure 3. Signal voltage in gauges (1) and (3) for a 300 kPa loading pulse.

From this formula the dynamic elastic modulii of the bars and of the specimen can be calculated using the equation:

$$E_{dyn} = \rho c^2 \tag{3}$$

3.2 *Converting voltage to strain*

The objective of the testing program is to study the dynamic behavior of the Lavasan granite at very high strain rates. It is therefore necessary to extract the stress-strain curve from the signals recorded by each gauge. Indeed, the strain gauges used consist of a Wheatstone bridge, which is characterized by a gauge factor κ.

The relationship between the resistance, R, and the longitudinal deformation undergone by the gauges can be determined by

$$\frac{\Delta R}{R} = \kappa \varepsilon_l \tag{4}$$

Therefore, it is possible to relate the supply voltage to the voltage measured in the longitudinal deformation, V_{ex}.

$$\varepsilon_l = \frac{2}{(1+\nu)\kappa}\frac{V_{out}}{V_{ex}} \tag{5}$$

where ε_l is longitudinal deformation of the bars, ν is Poisson's ratio, V_{out} is the output voltage and V_{ex} is the excitation in volts (20 V, ±0.1 V). For this case, the gauge factor was 2.115.

Figure 3 shows the output voltage with respect to time for both the incident and the reflected waves for a 300 kPa loading pulse.

3.3 *Stress in the specimen*

The average stress in the specimen can be expressed in terms of the forces applied on each surface of the specimen. A schematic representation of any specimen is shown in Figure 4.

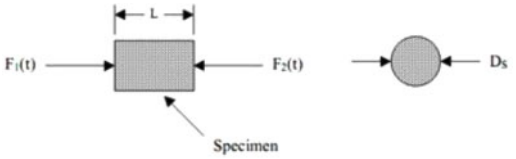

Figure 4. Schematic diagram of the cylindrical specimen.

When the specimen is sandwiched between the pressure bars, forces $F_1(t)$ and $F_2(t)$ are applied to the specimen of diameter D_s. The average force on the specimen is given by:

$$F_{AVG}(t) = \frac{F_1(t) + F_2(t)}{2} \tag{6}$$

Hence the average stress on the cylindrical specimen is computed by:

$$\sigma_{AVG}(t) = \frac{F_{AVG}(t)}{\pi D_s^2/4} \tag{7}$$

The stress at the contact surface between the specimen and the input and the output bars can be calculated using the formula:

$$\sigma_1(t) = E_b\left[\varepsilon_I(t) + \varepsilon_R(t+\Delta t)\right] \tag{8}$$

$$\sigma_1(t) = E_b\,\varepsilon_T(t) \tag{9}$$

where, $\varepsilon_I(t)$ is the incident strain wave, $\varepsilon_R(t)$ is reflected strain wave, $\varepsilon_T(t)$ is the transmitted strain wave and E_b is the elastic modulus of the bar (equation 3).

The forces $F_1(t)$ and $F_2(t)$ acting on the specimen surfaces are due to the pressure bars. For a specimen in dynamic equilibrium, the forces at the ends of the pressure bars may be expressed in terms of the incident and reflected pressure bar strains as follows:

$$F_1(t) = A_1.\sigma_1(t) = E\left[\varepsilon_I(t) + \varepsilon_R(t)\right]\frac{\pi D_b^2}{4} \tag{10}$$

$$F_1(t) = A_1.\sigma_T(t) = E\,\varepsilon_T(t)\,\frac{\pi D_b^2}{4} \tag{11}$$

Substituting equations (10) and (11) into equation (6) gives an expression for the average stress on the specimen in terms of the pressure bar strains:

$$\sigma_{AVG}(t) = \frac{E D_b^2}{2D_s^2}\left[\varepsilon_I(t) + \varepsilon_R(t) + \varepsilon_T(t)\right] \tag{12}$$

where D_b is the diameter of the pressure bars.

3.4 *Strain and strain rate in the specimen*

Particle velocity at the end of the input and output bars (V_{inc} and V_{tr}) can be calculated from the equations:

$$V_1(t) = C_{inc}\left[\varepsilon_I(t) - \varepsilon_R(t)\right] \tag{13}$$

Table 2. Geometry and material properties of SHPB components.

Properties	Striker*	I- bar**	T-bar***
Young modulus [Pa]	2e11	7.363e11	7.363e11
Density (kg/m^3)	7700	2810	2810
Poisson's ratio	0.3	0.3	0.3
Diameter [m]	0.05	0.05	0.05
Length (m)	900 (50)	3.0	2.0

*Steel
**Input bar (aluminum)
***Output bar (aluminum)

$$Vtr(t) = C_{inc}\,\varepsilon_T(t) \tag{14}$$

Then, the average strain rate of the specimen is given by equation (15):

$$\dot{\varepsilon}_m = \frac{V_T(t) - V_T(t)}{l_{spec}} \tag{15}$$

where, l_{spec} is the length of the specimen. For a point in the specimen, the strain is expressed as follows:

$$\dot{\varepsilon}_2 = \frac{\Delta\varepsilon}{\Delta t} = \frac{\varepsilon_2 - \varepsilon_1}{t_2 - t_1} \tag{16}$$

We can obtain the strain value at any instant in time based on the strain rate and the above strain value:

$$\varepsilon_2 = \varepsilon_1 + \dot{\varepsilon}_2\left(t_2 - t_1\right) \tag{17}$$

where t_1, t_2 are the times corresponding to the ε_1 and ε_2 values which are recorded by the gauges.

3.5 *Preliminary tests*

Initially, the bars were tested without any specimen to determine their own properties. The properties of the SHPB components are reported in Table 2. The location of each strain gauge pair on the bars is identified by a number. In this study, the gauges are located in the center of the bars.

4 SHPB TEST RESULTS

For experiments carried out on rock specimens, the loading pulse was progressively increased from 100 kPa to 350 kPa. Using a striker of 900 mm in length, the specimen was destroyed at a 350 kPa loading pulse.

The measured signal (60.000 values) allows one the computation of the dynamic elastic modulus of the specimen, which was found to be 76.5 GPa. The travel time of the striker, Δt, was equal to 3.26 μs for a pulse of 300 kPa. As the distance between two gauges is 50 mm, the velocity of the striker bar is 15.34 m/s (17.34 m/s for a pulse of 350 kPa).

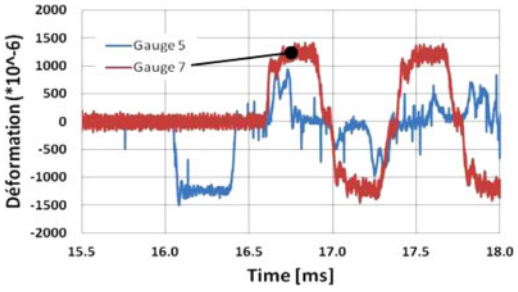

Figure 5. Strain of input bar (gauges 5) and output bar (gauge 7) versus time for a 300 kPa loading pulse (specimen 38).

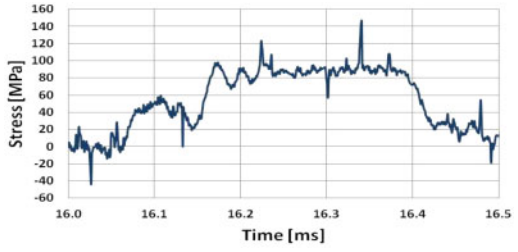

Figure 6. Stress in the input bar versus time for a 300 kPa loading pulse (specimen 38).

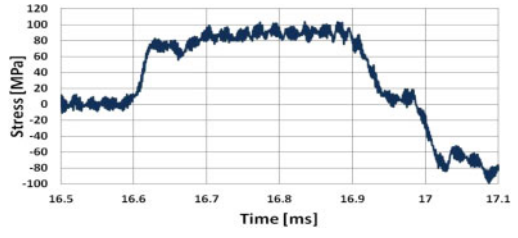

Figure 7. Stress in the output bar versus time for a 300 kPa loading pulse (specimen 38).

Using the signal measured by the gauges, and combining the above equations for the longitudinal deformation, the incident strain wave $\varepsilon_I(t)$, reflected strain wave $\varepsilon_r(t)$ and transmitted strain wave $\varepsilon_T(t)$ in the bars were calculated based on equation (5). Figure 5 shows the strains versus the time measured in both the input bar and the output bar.

From these results, the stress in the bars at the two contact surfaces $\sigma_I(t)$, $\sigma_T(t)$, as well as the average stress on the specimens were computed (eq. (12)). Using the particle velocity values at the end of input and output bars $V_I(t), V_T(t)$, the average strain rate and strain values of the specimen can also be determined by using the equations (15) and (17). Stresses in the input bar and the output bar are represented with respect to time in Figures 6 and 7. From these results, it can be clearly seen that the maximal stress values in the specimen increase when the loading pulse value is larger.

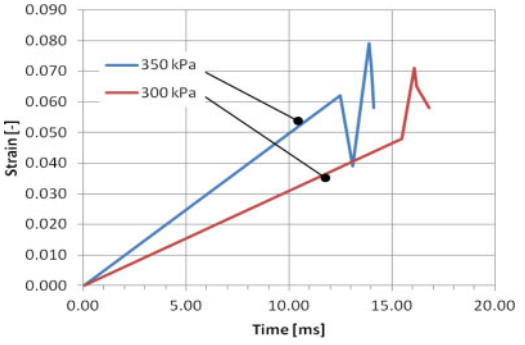

Figure 8. Strain versus time in specimen 38 for 300 kPa and 350 kPa loading pulse.

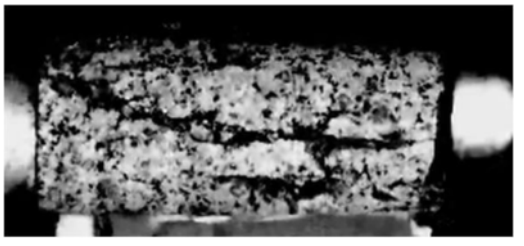

Figure 9. Photo of a specimen after failure; a longitudinal fracture can clearly be seen after the strike.

The relationships between stress and strain in specimen 38 for the 300 kPa and 350 kPa loading pulses are presented in Figure 8. As the force applied by the striker bar is proportional to its velocity, an increase in the velocity increases both the strain and the strain rate in the specimen.

Figure 9 shows a photo of the specimen after failure; a longitudinal fracture can clearly be seen after the strike.

Additional tests were performed with a shorter striker and a higher pulse pressure (up to 500 kPa). The goal was to reduce the time during which the load is applied to the specimen in order to be closer to the in situ conditions for tunnel blasting.

When using a shorter striker (50 mm in length instead of 900 mm) it was found that the duration of load application is reduced, dropping from 350 μs to 50 μs. Consequently, the dynamic strength of the specimen is substantially increased up to 205 MPa.

5 PRELIMINARY NUMERICAL SIMULATIONS OF SHPB TESTS

In order to determine the efficiency of blasting for tunnel excavation in granite, some numerical simulations of the SHPB tests were performed using the Finite Element code ABAQUS/Explicit (Abaqus, 2010). The material properties of bars used in the SHPB tests were presented in Table 2. A 3-D axisymmetric model of the SHPB was built using 8-node brick elements

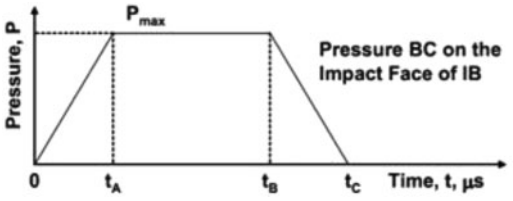

Figure 10. Loading pulse history on the impacted face of the input bar.

(C3D8R). The longitudinal axis of the bars is the z-axis.

A surface contact interface condition without friction is defined between the bar-specimen interfaces. The displacements of bars in X- and Y-axes (cross section) and in the end face of the output bar were assumed to be zero. The specimen is represented as a circular cylinder. The bars remain elastic at all times during the SHPB experiments, and therefore can be considered as a linear-elastic isotropic material. The specimens are modeled with a linear-elasto-plastic constitutive law using a Mohr-Coulomb failure criterion whose parameters were deduced from the properties given in Table 1.

The input bar is divided into 6240 elements (approximate global size 0.02). The number of elements in the output bar is 3900 (approximate global size 0.02). The approximate global size of the specimen element is chosen to be smaller (0.015); it is therefore divided into 129 elements. The total number of elements in this model is 10255 with 13024 nodes.

The impact velocity of the striker is converted to a pressure pulse applied on the impact face of the input bar. The pressure applied to the face is introduced directly in the form of a slot as shown in Figure 10. Its magnitude is given by:

$$P_{max} = \frac{1}{2}\rho\ S_b\ C\ V_{st} \tag{18}$$

where ρ is the density of the striker, S_b is the section of the bars, C is the velocity of wave propagation in the striker (equation 2), V_{st} is the velocity of the striker bar (17.34 m/s in the case of a 350 kPa pressure pulse).

The duration of the application of the force is a function of the striker length. The stress pulse applied to the input bar is defined using the four parameters: t_A, t_B, t_C and $P_{max.}$

In this study, the time parameters were chosen as follows: $t_A = 99$ μs, $t_B = 101$ μs, $t_C = 200$ μs, $T = 200$ μs. The amplitude of the loading pulse, calculated using equation (18), is equal to $P_{max} =$ 34234052 Pa.

The results of the SHPB numerical simulation are presented in Figures 11, 12 and 13. The comparison of the numerical results to the experimental results shows good agreement for the stresses and strains in the specimen despite the fact that the computed maximum stress is smaller than the value obtained from the tests.

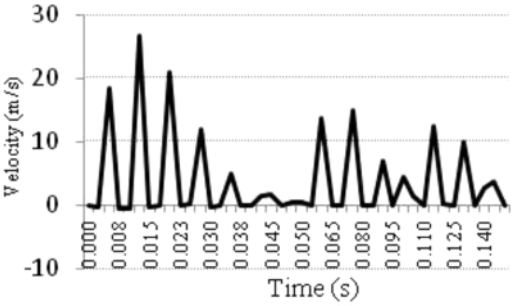

Figure 11. Particle velocity versus time in the input bar.

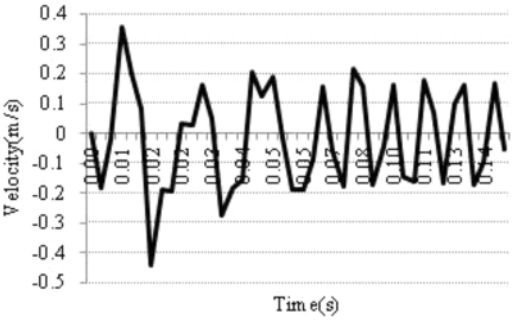

Figure 12. Particle velocity versus time in the output bar.

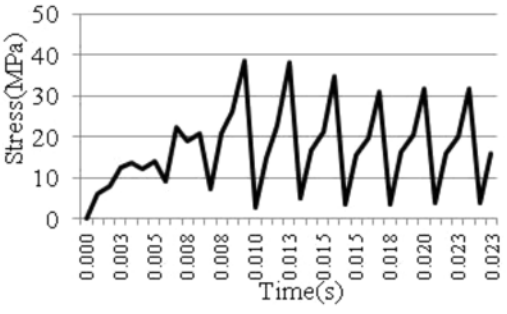

Figure 13. Stress versus time in the specimen.

The reason for this discrepancy may be due to imperfect contact at the interfaces between the bars and the specimen. Another issue is related to the boundary condition of the bar: In the model, displacements were assumed to be equal to zero at the end of the bar. This is not necessarily true in the experiments.

6 CONCLUSIONS

This study allows us to highlight the effect of dynamic loading on the mechanical properties of Lavasan granite. It was found that both the uniaxial compressive strength (UCS) and Young's modulus substantially increase with the rate of loading. It was also observed that the duration of the loading depends on the length of the striker; the longer the striker the larger the loading time and therefore is the lower the UCS. Additional tests are therefore required to assess this effect. The results of numerical modeling show that it is possible to compute realistic strain and stress in the rock specimen. This approach will be extended in the future to model the entire tunnel excavation process.

REFERENCES

ABAQUS, 2010. Getting Started with ABAQUS Version 6.10, ABAQUS, Inc.

Bohloli, B. 1997. Effects of the geological parameters on rock blasting using the Hopkinson split bar. International Journal of Rock Mechanics and Mining Sciences. 34: 32.e1–32.e9.

Forquin, P. Safa, K. Gary, G. 2010. Influence of free water on the quasi-static and dynamic strength of concrete in confined compression tests. Journal of Cement and Concrete Research. 40: 321–333.

Hopkinson, B. 1914. A method of measuring the pressure produced in the detonation of high explosives or by the impact of bullets. Philosophical Transactions of the Royal Society (London) A. 213: 437–456.

Johnson, J.C. 2010. The Hustrulid bar – a dynamic strength test and its application to the cautious blasting of rock. PhD Thesis, University of Utah.

Kaiser, M.A. 1998. Advancements in the Split Hopkinson Bar Test, Master of Science in Mechanical Engineering – Virginia Tech University, Blacksburg, Virginia.

Keshavarz, M. Pellet, F.L. Amini Hosseini, K. Rousseau, C. 2008. Comparing the results of acoustic emission monitoring in Brazilian and uniaxial compression tests. Proc. 5th Asian Rock Mechanics Symposium, Tehran, Iran: 357–363.

Keshavarz, M. Pellet, F.L. Amini Hosseini, K. 2009. Effectiveness of energy and hit rate parameters of acoustic emission for prediction of rock failure. Proc. Sinorock Symposium, Hong Kong, China, CDRom.

Kolsky, H. 1949. An investigation of the mechanical properties of materials at very high rates of loading. Proceedings of the Physical Society of London, B62: 676–700.

Pellet, F. L. Keshavarz, M. Amini Hosseini, K. 2011. Mechanical damage of a crystalline rock having experienced ultra high deviatoric stress up to 1.7 GPa. International Journal of Rock Mechanics and Mining Sciences. 48: 1364–1368.

Weimin, L. Jinyu, X. 2009. Impact characterization of basalt fiber reinforced geopolymeric concrete using a 100-mm-diameter split Hopkinson pressure bar, Journal Materials Science and Engineering. A 513–514: 145–153.

Zhou, Y.X. Xia, K. Li, X.B. Li, H.B. Ma, G.W. Zhao, J. Zhou, Z.L. Dai, F. 2012. Suggested methods for determining the dynamic strength parameters and mode-I fracture toughness of rock materials. International Journal of Rock Mechanics and Mining Sciences. 49: 105–112.